

# Lorentz Accelerations in the Earth Flyby Anomaly

Justin A. Atchison\* and Mason A. Peck†  
*Cornell University, Ithaca, New York, 14850*  
 and  
 Brett J. Streetman‡  
*Draper Laboratory, Cambridge, Massachusetts 02139*

DOI: 10.2514/1.47413

Mission engineers have detected an unexpected anomaly on six spacecraft during low-altitude gravity-assist maneuvers around Earth. This Earth flyby anomaly involves an acceleration that, to date, researchers cannot account for based on known forces or errors in measurement or modeling. This paper evaluates Lorentz accelerations associated with spacecraft electrostatic charging as a possible explanation for the Earth flyby anomaly. This analysis does not explicitly address plasma physics but, instead, bases its conclusions on fundamental six-state flight dynamics. The analysis focuses on the Near Earth Asteroid Rendezvous spacecraft, because it exhibited the largest anomalous error with the smallest estimated residuals. The analysis takes the form of a boundary-value problem in which vector-disturbance time histories are found numerically through nonlinear optimization methods. The analysis identifies the unknown, but required, acceleration based on a model of the Lorentz-force interaction. The algorithm cannot converge on a solution that fully reproduces the anomalous error in all six orbital states. It is unlikely, based on this analysis, that Lorentz forces cause the flyby anomaly.

## Nomenclature

$a_i$	= $i$ th cosine coefficient in a Fourier series
$\mathbf{B}$	= magnetic field
$b_i$	= $i$ th sine coefficient in a Fourier series
$E$	= eccentric anomaly
$e$	= eccentricity
$\mathbf{F}_L$	= Lorentz force
$g_i$	= perturbation accelerations projected onto $\hat{i}$
$H(t)$	= Heaviside step function
$h$	= orbital angular momentum
$i$	= inclination
$\mathbf{J}$	= vector cost function
$K$	= unitless constant
$M$	= mean anomaly
$m$	= spacecraft mass
$q$	= net electrostatic charge
$\mathbf{r}$	= spacecraft position vector with magnitude $r$ and direction $\hat{r}$
$t$	= time
$\mathbf{v}$	= spacecraft velocity vector
$v_{\text{inf}}$	= hyperbolic excess velocity
$v_{\text{rel}}$	= spacecraft velocity relative to $\mathbf{B}$
$\mathbf{W}$	= cost function weighting matrix
$\mathbf{X}$	= spacecraft orbital state vector
$x, y, z$	= Cartesian coordinates aligned with the geocentric equatorial inertial system
$\mathbf{X}_2$	= simulated charged spacecraft state after close approach
$\mathbf{X}_2^0$	= predicted spacecraft state after close approach
$\mathbf{X}_2^*$	= first observed spacecraft state after close approach

Presented as Paper 6000 at the AIAA Guidance, Navigation and Control Conference and Exhibit, Chicago, IL, 10–13 August 2009; received 28 September 2009; revision received 22 January 2010; accepted for publication 28 January 2010. Copyright © 2010 by Justin Atchison. Published by the American Institute of Aeronautics and Astronautics, Inc., with permission. Copies of this paper may be made for personal or internal use, on condition that the copier pay the \$10.00 per-copy fee to the Copyright Clearance Center, Inc., 222 Rosewood Drive, Danvers, MA 01923; include the code 0731-5090/10 and \$10.00 in correspondence with the CCC.

\*Graduate Research Assistant, Sibley School of Mechanical and Aerospace Engineering, 245 Upson Hall. Student Member AIAA.

†Assistant Professor, Sibley School of Mechanical and Aerospace Engineering, 212 Upson Hall. Member AIAA.

‡Senior Member of Technical Staff, Draper Laboratory. Member AIAA.

$\Gamma(t)$	= truncated Fourier series approximation of a function of time
$\delta_i$	= declination angle of incoming spacecraft velocity vector
$\delta_o$	= declination angle of outgoing spacecraft velocity vector
$\varepsilon$	= orbital energy
$\theta$	= azimuthal angle, measured from the + $x$ axis
$\mu$	= geocentric gravitational constant
$\nu$	= true anomaly
$\Pi(t)$	= boxcar shape function
$\rho^0$	= observed state errors associated with anomaly
$\tau$	= time constant of basis function
$\phi$	= colatitudes angle, measured from the + $z$ axis
$\Omega$	= longitude of the ascending node
$\omega$	= argument of perigee
$\omega_B$	= vector spin rate of the magnetic field

## I. Introduction

NEARLY every deep-space mission of the past 30 years has used a gravity-assist maneuver, or flyby, to achieve low-cost  $\Delta v$ . Gravity-assists enabled Voyager 1 to depart the solar system, Apollo 13 to return to Earth safely from the moon, Galileo to tour the Jovian moon system, and Ulysses to view the sun's polar regions. These maneuvers capitalized on the physics of three-body dynamics to transfer energy and momentum between a planet and a spacecraft in a heliocentric reference frame. These physics have been understood in terms of the restricted three-body problem for nearly two centuries.

It was therefore surprising when, in 1990, engineers at the Jet Propulsion Laboratory observed an energy change in the Galileo spacecraft's Earth gravity-assist (EGA) maneuver that could not be explained [1,2]. At the spacecraft's close approach to Earth, radar tracking stations were unable to slew quickly enough to follow Galileo's trajectory. When the acquisition of radar data resumed, tracking indicated that the spacecraft had experienced an unexplained acceleration that resulted in an orbit different from what had been predicted. After detecting this anomaly, researchers began a systematic study to identify what has come to be known as the flyby anomaly and identify its potential causes.

Since that initial observation, mission engineers have observed five other anomalous EGAs. Table 1 reproduces relevant values for the anomalous EGAs [2]. The details vary among these gravity-assist

**Table 1** Anomalous flyby parameters<sup>a</sup> (MESSENGER denotes Mercury surface, space environment, geochemistry, and ranging spacecraft)

Spacecraft	Galileo	Galileo	NEAR	Cassini	Rosetta	MESSENGER
Date of flyby	08 Dec. 1990	08 Dec. 1992	23 Jan. 1998	18 Aug. 1999	04 March 2005	02 Aug. 2005
Mass, kg	2497	2497	730	4612	2895	1086
Altitude of perigee, km	960	303	539	1175	1956	2347
Inclination, deg	142.9	138.7	108.0	25.4	144.9	133.1
Turn angle, deg	47.7	51.1	66.9	19.7	99.3	94.7
Velocity at perigee, km/s	13.740	14.080	12.739	19.026	10.517	10.389
$v_{\text{inf}}$ , km/s	8.949	8.877	6.851	16.010	3.863	4.056
Anomalous $\Delta v_{\text{inf}}$ , mm/s	3.92	-4.6	13.46	-2	1.80	0.02
Error bound for $\Delta v_{\text{inf}}$ , mm/s	0.3	1.0	0.01	1	0.03	0.01

<sup>a</sup>Data courtesy of Anderson et al. [2].

maneuvers, but they all share an unexplained acceleration. Although the anomalous acceleration produces a change in all of the orbital states, it is often described as a change in the hyperbolic excess velocity  $v_{\text{inf}}$ . In the six known cases,  $v_{\text{inf}}$  has been observed to both increase and decrease with magnitudes on the order of millimeters per second. Four additional EGAs with high-altitude close approaches have not shown anomalous energy changes. So, some infer a correlation with distance.<sup>§</sup>

Researchers have ruled out measurement errors as a cause of the flyby anomaly and have determined that the acceleration is a physical phenomenon: a variety of instruments and algorithms have detected the acceleration for the different spacecraft and orbits [2]. In addition, radar measurements have confirmed the anomaly by using both Doppler and time-of-flight range data. Researchers have proposed and evaluated a wide range of possible causes for the flyby anomaly [3–5]. Antreasian and Guinn have shown that the anomaly cannot be produced by a conservative field only, and the unknown acceleration may vary in time [6].

Anderson et al. recently reported that the magnitude of the anomaly correlates with the cosine of the declination of the spacecraft's incoming  $\delta_i$  and outgoing  $\delta_o$  velocity vectors [2]:

$$\frac{\Delta v_{\text{inf}}}{v_{\text{inf}}} = K(\cos \delta_i - \cos \delta_o) \quad (1)$$

The unitless constant  $K$  is empirically calculated to match the known data points, although it can be related to known Earth constants. Two papers explore Eq. (1) as a consequence of an unknown force field. Hasse et al. conclude that any candidate force field would contain a dependence on the velocity of the spacecraft [7]. Lewis finds that a quadrupole scalar potential field could produce this fit, and it would relate to a coupling of kinetic energies between the Earth and the spacecraft [8].

Since Anderson et al.'s finding [2], a variety of specific explanations have been proposed. These address reassessments of general and special relativity [9–13], the number of dimensions of space [14], dark matter somehow bound to Earth [15,16], the Casimir effect [17,18], and the concept of privileged frames [19]. To date, the research community has not yet accepted any of these studies as an adequate explanation for the flyby anomaly.

Five specific observations motivate evaluation of Lorentz forces associated with spacecraft charging as a source of the anomaly. The Lorentz force is based on well-understood physics: it has been observed in the orbital dynamics of dust particles at Jupiter [20–22] and Saturn [23,24]. The Lorentz force is nonconservative transferring energy between the Earth's rotating magnetic field and the charged spacecraft's orbit [25]. This transfer can either increase or decrease the energy of a spacecraft's orbit. The Lorentz force is distance-dependent, varying with  $r^{-7/2}$ . Finally, simulated Lorentz maneuvers at Earth show a strong correlation between declination and energy change [26].

In their review of a number of unexplained physical phenomena, Lammerzahl et al. address the problem of the Earth flyby anomaly.

In a brief paragraph, the authors dismiss the Lorentz force using simple order-of-magnitude estimates [4]

In a recent study of charging of the LISA test masses [27], the charging has been estimated by  $10^{-10}$  C. So, for the whole satellite, it might be a conservative assumption that the charge is less than  $Q \leq 10^{-7}$  C. A satellite of 1 t carrying a charge  $Q$  and moving with  $v = 30$  km/s in the magnetic field of the Earth, which is of the order 0.2 G, will experience an acceleration  $10^{-8}$  m/s<sup>2</sup> far below the observed effect.

Their analysis rules out the Lorentz force on the basis of a priori estimates of spacecraft charge. In contrast, the objective of the present work is to investigate the problem without presupposing a certain charge magnitude. Instead, it is based on a full vector mechanics representation of the physics. Furthermore, previous research has explored the possibility of generating electrostatic charge on spacecraft to achieve novel spacecraft maneuvers [25,26,28,29], including augmented flybys [30]. This work has shown that the Lorentz force can generate meaningful acceleration on a spacecraft. The present study begins from first principles to investigate the possibility that a spacecraft with any electrostatic charge can recreate these anomalous behaviors, regardless of magnitude, sign or variation in time. Put simply, the spacecraft charge is an output of this analysis, not an input.

This analysis addresses this question in the context of a test case, the Near Earth Asteroid Rendezvous (NEAR) spacecraft, using original data. This spacecraft demonstrated the greatest anomaly with the lowest error residuals of all the examples, and it is therefore the best candidate to address. Demonstrating that Lorentz accelerations can explain NEAR's anomalous orbit time history is necessary, but not sufficient, evidence for explaining the others.

## II. Modeling and Analysis

A spacecraft with an electrostatic charge  $q$ , moving with velocity  $\mathbf{v}_{\text{rel}}$  relative to a magnetic field  $\mathbf{B}$ , experiences the Lorentz force  $\mathbf{F}_L$

$$\mathbf{F}_L = q\mathbf{v}_{\text{rel}} \times \mathbf{B} \quad (2)$$

For a rotating magnetic field

$$\mathbf{v}_{\text{rel}} = \dot{\mathbf{r}} - \boldsymbol{\omega}_B \times \mathbf{r} \quad (3)$$

$\dot{\mathbf{r}}$  is the vector time derivative of the spacecraft's position  $\mathbf{r}$  (with magnitude  $\mathbf{r}$  and direction  $\hat{\mathbf{r}}$ ) relative to the system's barycenter in a Newtonian frame, and  $\boldsymbol{\omega}_B$  is the angular velocity of the magnetic field.

The spacecraft's orbital state determines the value for every term in these expressions except for the scalar  $q$ . Thus, the direction of the Lorentz force is confined to a one-dimensional manifold corresponding to varying charge magnitude. Figure 1 shows the line of action for the blackout time of NEAR at 3 min increments along the orbital path. The spacecraft approaches Earth from the  $+z$  direction and makes its closest approach above the Middle East. The direction of  $\mathbf{v}_{\text{rel}} \times \mathbf{B}$  is nearly constant before the close approach and again after the close approach. At closest approach,  $\mathbf{v}_{\text{rel}} \times \mathbf{B}$  lies in a predominantly cross-track direction, after which it rotates to an along-track direction. Figure 2 shows the magnitude of  $\mathbf{v}_{\text{rel}} \times \mathbf{B}$

<sup>§</sup>Personal communication with John D. Anderson of the Jet Propulsion Laboratory, on 23 January 2009.

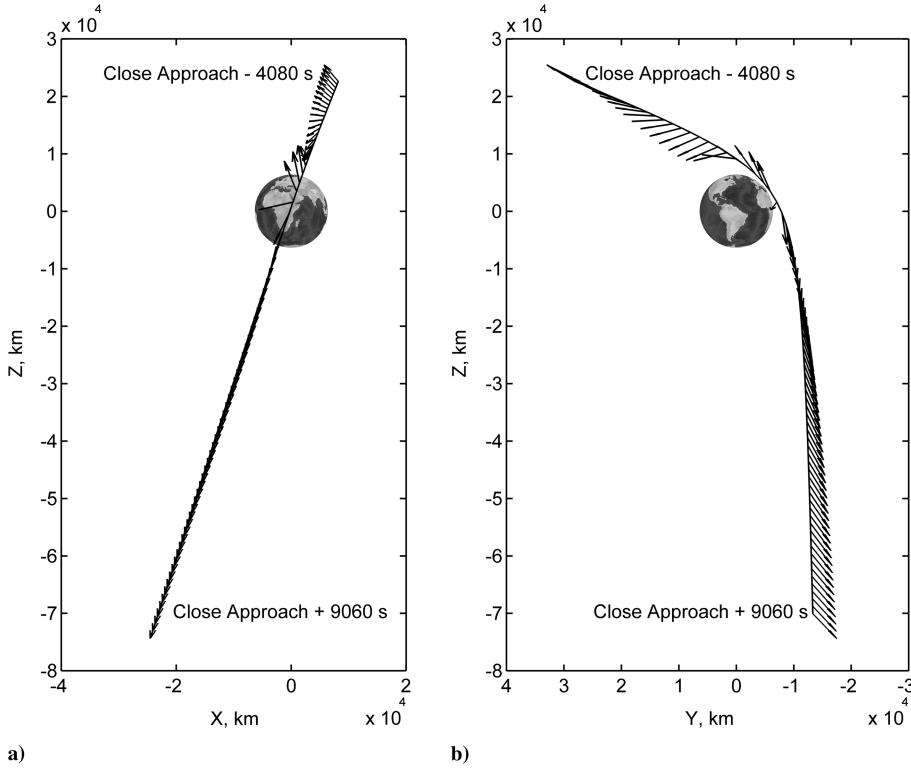
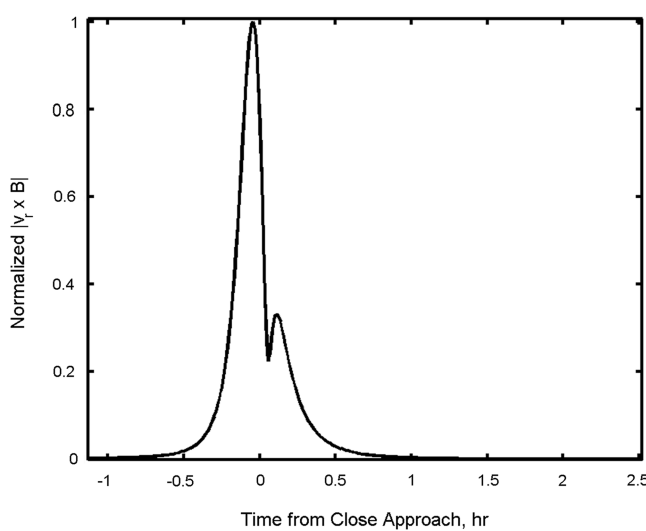


Fig. 1 The direction of  $(v_{\text{rel}} \times B)$  for the NEAR EGA during the data-blackout period shown from a) the eastern hemisphere and b) the western hemisphere.

versus time over the data-blackout period, in which the vector magnitude is normalized by the maximum value. The magnitude is largest near close approach, where both  $|v_{\text{rel}}|$  and  $|B|$  are maximized. This magnitude quickly drops off, leaving only a 1 h window in which the Lorentz force can be of any significance.

The following two-body equations of motion represent the Lorentz force in terms of spherical coordinates:

$$\begin{aligned}\ddot{r} &= r\dot{\theta}^2 \sin^2\phi + r\dot{\phi}^2 - \frac{\mu}{r^2} + g_r + \left( \frac{F_L}{m} \cdot \hat{\mathbf{r}} \right) \\ r\ddot{\phi} &= -2\dot{r}\dot{\phi} + r\dot{\theta}^2 \sin\phi \cos\phi + g_\phi + \left( \frac{F_L}{m} \cdot \hat{\phi} \right) \\ r \sin\phi \ddot{\theta} &= -2\dot{r}\dot{\theta} \sin\phi - 2r\dot{\phi}\dot{\theta} \cos\phi + g_\theta + \left( \frac{F_L}{m} \cdot \hat{\theta} \right)\end{aligned}\quad (4)$$



**Fig. 2** The normalized magnitude of  $(v_{\text{rel}} \times B)$  for the NEAR EGA during radar blackout.

where the coordinates and axes are given in Fig. 3. The terms  $g_r$ ,  $g_\phi$ , and  $g_\theta$  are perturbation accelerations along each axis. The model for the present analysis includes accelerations due to high-order gravitational terms ( $100 \times 100$  EGM96); direct and indirect accelerations associated with the sun, moon, Jupiter, and Venus; solar radiation pressure; relativity (point-mass and Lense-Thirring effects); and atmospheric drag. Accelerations associated with Earth albedo, Earth infrared, ocean tides, indirect oblateness, moon oblateness, and the remaining planets are negligible. (For a review of these effects for the NEAR and Galileo EGAs, see [6].) In spite of these omissions, the model recreates the published value of anomalous  $\Delta v_{\text{inf}}$  to within 0.01%. The magnetic field  $\mathbf{B}$  is modeled with a  $10 \times 10$  spherical harmonic representation of the International Geomagnetic Reference Field for 1995. In each Eq. (3),  $\frac{\mathbf{F}_L}{m}$  represents the acceleration imparted by the Lorentz force.

The scalar hyperbolic excess energy is

$$v_{\text{inf}}^2 = \mathbf{v} \cdot \mathbf{v} - \frac{2\mu}{r} \quad (5)$$

A complete evaluation of the anomaly addresses the transition of six orbital states  $X$  during the flyby rather than simply representing the

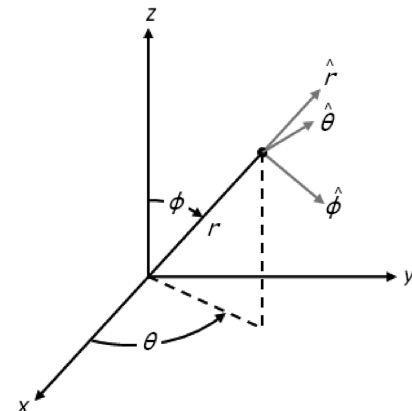


**Fig. 3** Spherical coordinates and axes.

**Table 2** Polarity and magnitude of anomalous state change for NEAR

GEI cartesian coordinates		GEI spherical coordinates		Orbital elements	
<i>x</i>	$+10^2$ m	<i>r</i>	$-10^2$ m	$\varepsilon$	$+10^2$ J/kg
<i>y</i>	$-10^3$ m	$\phi$	$-10^{-7}$ rad	<i>h</i>	$+10^5$ m <sup>2</sup> /s
<i>z</i>	$+10^2$ m	$\theta$	$+10^{-6}$ rad	<i>e</i>	$+10^{-6}$
$\dot{x}$	$-10^{-3}$ m/s	$\dot{r}$	$+10^{-2}$ m/s	<i>i</i>	$-10^{-6}$ rad
$\dot{y}$	$-10^{-3}$ m/s	$\dot{\phi}$	$+10^{-10}$ rad/s	$\Omega$	$-10^{-6}$ rad
$\dot{z}$	$-10^{-2}$ m/s	$\dot{\theta}$	$+10^{-11}$ rad/s	$\omega$	$-10^{-8}$ rad
				<i>v</i>	$-10^{-6}$ rad
				<i>M</i>	$+10^{-5}$ rad
				<i>E</i>	$-10^{-6}$ rad

difference in energy, a mere scalar that cannot represent the full subtlety of the problem.  $X$  can be expressed, for example, in Cartesian coordinates taken in the geocentric equatorial inertial (GEI) frame [ $x, y, z, \dot{x}, \dot{y}, \dot{z}$ ], spherical coordinates as described in the equations of motion [ $r, \phi, \theta, \dot{r}, \dot{\phi}, \dot{\theta}$ ], or Earth-centered classical orbital elements [ $a, e, i, \Omega, \omega, v$ ]. Table 2 shows the observed anomalous change in each of these representations of the six states.

Perturbation techniques can map the changes associated with the Lorentz force throughout NEAR's orbit into these various coordinates. Then, general perturbation equations shown in equations 9–24 of [31], transform the change into orbital elements. Figure 4 shows the accumulated changes for nine such coordinates for a constant positive  $q/m = +1$  mC/kg, an arbitrary example. (The polarity of  $q/m$  appears linearly in the calculation of  $F_L$ , so a negatively charged spacecraft produces the opposite of the changes observed in Fig. 4.) Three elements ( $\Omega, \omega, M$ ) show monotonic change throughout the flyby. Comparing these results with Table 2 leads to the conclusion that the charge-to-mass ratio of the spacecraft must be negative at some point to produce the observed anomaly. These results offer no further insight beyond this single observation; one cannot rule out the Lorentz force solely on the basis of a single constant charge.

### III. Numerical Approach

Since the results of the perturbation analysis are inconclusive, this research turns to numerical optimization methods for nonlinear systems. In this context, the anomaly is treated as an optimization problem with known boundary values; seeking to solve for a  $q(t)$  that

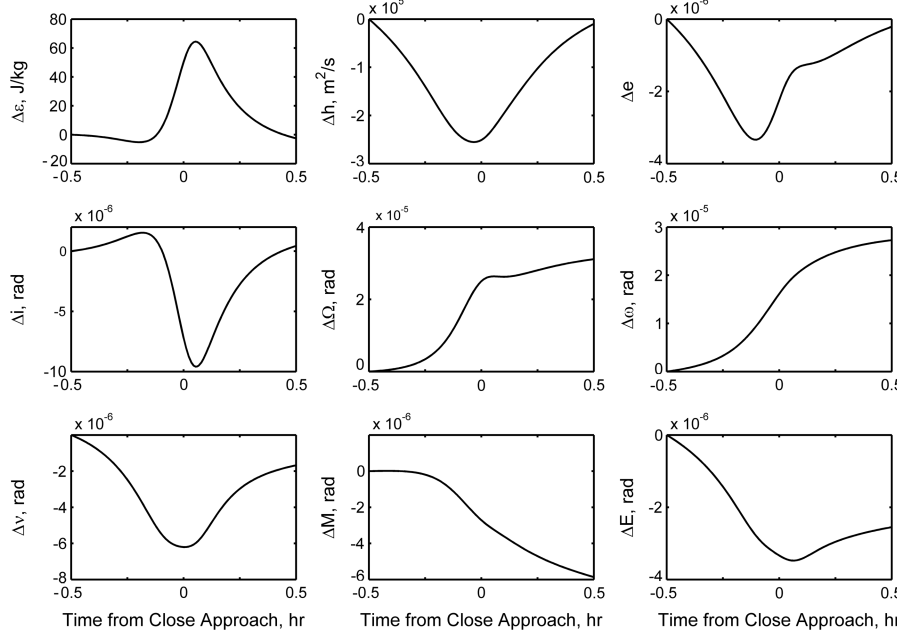


**Fig. 4** Accumulated change in orbital elements associated with a constant positive charge-to-mass ratio of 1 mC/kg for a 1 h window around closest approach.

can evolve from the last known state before the radar blackout  $X_1$  to the first known state after the radar blackout  $X_2^*$ . Figure 5 illustrates these states with exaggerated orbits.  $X_2^0$  is the predicted state, found by propagating  $X_1$  forward in time without any anomalous acceleration. The optimizer is meant to find a charge time history using an algorithm that minimizes a cost associated with the anomalous state errors. For this analysis, the cost is the weighted vector difference between the known postencounter state  $X_2^*$  and the postencounter state  $X_2$  simulated with a nonzero  $q(t)$  time history:

$$\mathbf{J} = \mathbf{W}[X_2^* - X_2] \quad (6)$$

$$\mathbf{J} = \|\mathbf{J}\| \quad (7)$$

The weighting matrix  $\mathbf{W}$  is diagonal with coefficients consisting of the inverse of the absolute value of the errors  $\rho^0$ :

$$\rho^0 = X_2^* - X_2 \quad (8)$$

$$\mathbf{W} = \frac{1}{\sqrt{6}}(\text{diag}|\rho^0|)^{-1} \quad (9)$$

This form normalizes the relative magnitudes of the components of  $\mathbf{J}$ , yielding a baseline cost for the uncharged spacecraft  $J^0$  of 1.0. Values for  $\rho^0$  are given in three coordinate systems in Table 2. Although the three systems—Cartesian, spherical, and classical orbital—are equivalent in the sense that the physics is independent of basis,  $X$  is expressed in a Cartesian-coordinate system for the cost modeling because its matrix expressions tend to be better conditioned than corresponding expressions in the other two systems.

A Fourier series serves as a basis to model the unknown acceleration. With enough terms, this basis can represent an arbitrary, continuous time history. Here, the series is truncated to some numerically manageable order,  $n$ . The Fourier series of an arbitrary function can be expressed as

$$\Gamma(t) = a_0 + \sum_{i=1}^n \left[ a_i \cos\left(\frac{2\pi i}{\tau} t\right) + b_i \sin\left(\frac{2\pi i}{\tau} t\right) \right] \quad (10)$$

$$a \in \mathbb{R}^{(n+1) \times 1}, \quad b \in \mathbb{R}^{n \times 1}$$

The parameters  $a_i$  and  $b_i$  describe the shape of  $\Gamma(t)$ , and  $\tau$  sets the length of the longest period. For an order  $n$  Fourier series, the

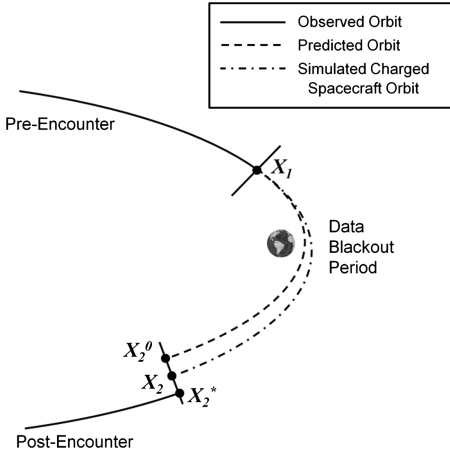


Fig. 5 Diagram of state definitions.

algorithm must optimize over  $2n + 1$  coefficients. Figure 6 shows a sample of four functions that are approximated with a sixth-order ( $n = 6$ ) Fourier series. This shape function captures a line with constant slope, a Heaviside step, and a triangular wave, all with accuracy acceptable for this application. However, it is much less effective at modeling an impulse function. To accommodate this limitation this study also considers a boxcar basis function, which describes a single “on” period of a square wave

$$\Pi(t) = c_0(H[t - t_0] - H[t - (t_0 + \Delta t)]) \quad (11)$$

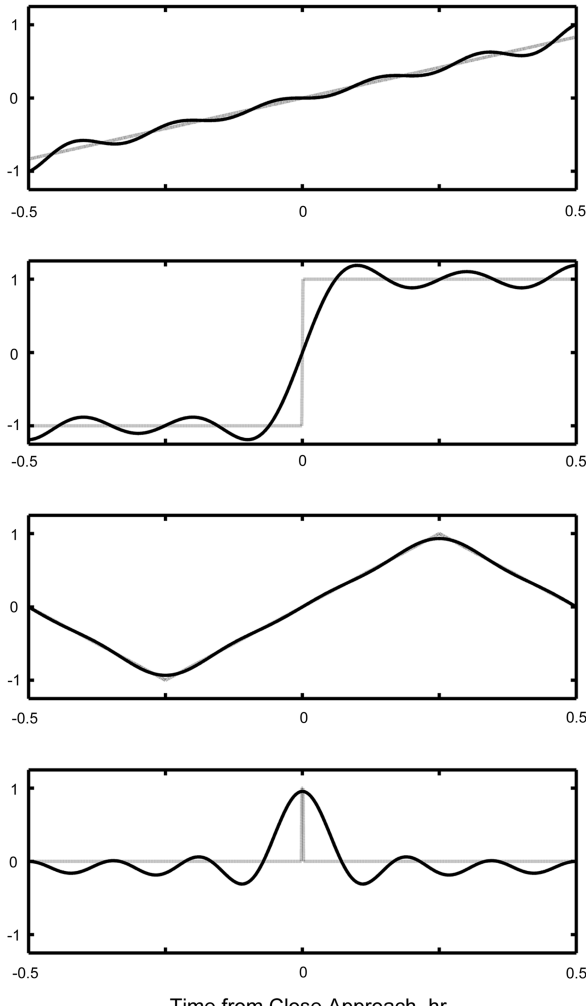


Fig. 6 Sample functions (dotted lines) approximated by a sixth-order Fourier series (solid lines).

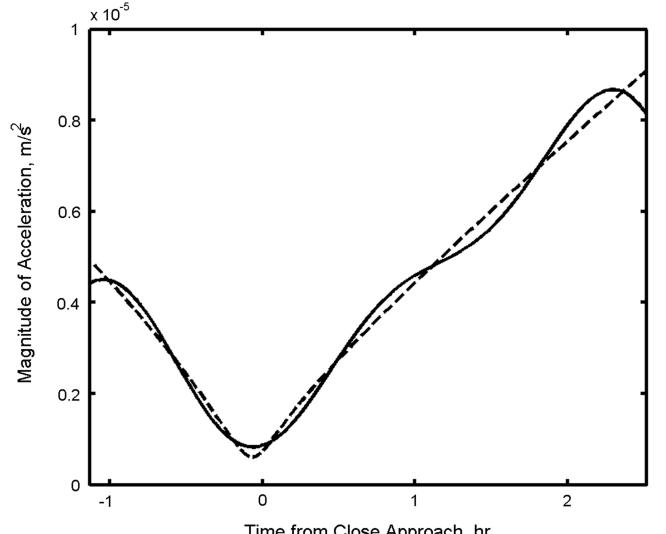


Fig. 7 Magnitude of acceleration due to the moon (dotted line), solved for by using the optimization algorithm (solid line).

$H(t)$  is the Heaviside step function. The parameters  $c_0$ ,  $t_0$ , and  $\Delta t$  set the function’s magnitude, start time, and pulse width, respectively. If  $\Delta t$  is sufficiently small, this shape function can approximate a single impulse. These two shape functions model both the unknown acceleration and the proposed  $q(t)$  time history.

MATLAB’s nonlinear least-squares optimization function lsqnonlin offers good convergence and repeatability for this application. This function uses a Levenberg–Marquardt line search method to estimate a local gradient and march toward a minimum cost  $J$  by varying the coefficients ( $a_i$ ,  $b_i$ ) that define  $q(t)$ . The change in step size defines the convergence. A threshold of  $10^{-14}$  yields sufficiently accurate solutions in this analysis with acceptable computation time. There are no guarantees that the resulting minimum is global rather than simply local. So, each optimization is based on a large and varying set of initial guesses.

To verify this numerical approach, one can test the algorithm with a known acceleration time history. As an example, the uncharged orbit from  $X_1$  through the data-blackout period is simulated with and without the presence of the moon’s accelerations.  $X_2^*$  becomes the postencounter state accounting for the moon, and  $X_2^0$  becomes the postencounter state excluding the moon. The algorithm then solves for the missing known acceleration given only the direction of the moon and modeling the magnitude of the acceleration as an eighth-order Fourier series. This test mimics the proposed Lorentz simulation in which the direction of  $v_{\text{rel}} \times \mathbf{B}$  is known, and the time-varying magnitude of  $q(t)$  is unknown.

The minimized cost  $J = 10^{-9}$  suggests that the algorithm modeled the missing acceleration associated with the moon with an acceptable precision, because such a cost indicates residual error in all states that is orders of magnitude lower than the observational error. Figure 7 shows the true and modeled magnitude of acceleration throughout the data-blackout period. The true lunar acceleration is similar to a portion of a triangle wave. The Fourier series approximation oscillates around the actual acceleration, with errors that are most noticeable near the two endpoints and the inflection point. However, the fact that the cost is based on an integrated time history allows these small errors to occur without significant impact. A higher-order approximation reduces these errors at the cost of computation time.

#### IV. Results

Before solving for an optimized  $q(t)$  time history, the algorithm is used to test for the existence and uniqueness of an arbitrary continuous or impulsive solution to the given boundary-value problem. With a well-posed question, the algorithm is then used to search for a  $q(t)$  time history.

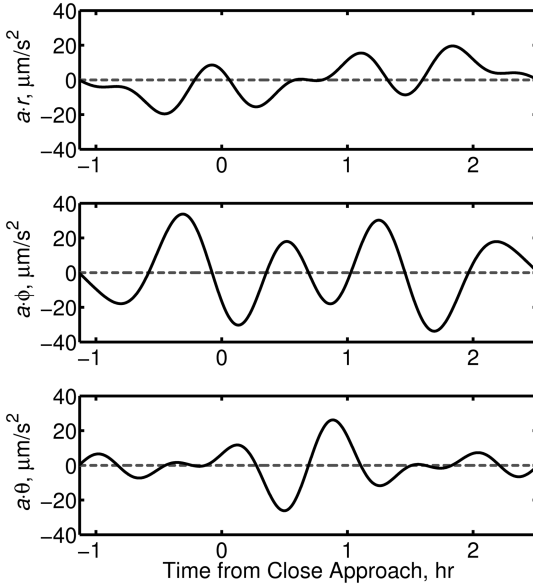


Fig. 8 Sample continuous acceleration that reproduces the anomaly, shown in  $\hat{r}$ -,  $\hat{\phi}$ -, and  $\hat{\theta}$ -aligned components.

#### A. Existence and Nonuniqueness of a Continuous Solution

For there to be a physical explanation for the anomaly, a continuous solution must exist for the boundary-value problem. With  $X_2^*$  as the observed postencounter state and  $X_2^0$  as the predicted postencounter state, the optimization can determine whether any physically realizable solution exists (regardless of the cause). For this analysis, three sixth-order Fourier series aligned with the  $\hat{r}$ ,  $\hat{\phi}$ , and  $\hat{\theta}$  directions model the unknown acceleration. Setting the sum of the cosine terms in the Fourier series to zero ensures that the applied force is zero at the boundary points. This boundary condition reflects the fact that the anomaly occurs within the data-blackout period and that the forces are known both before and after the blackout. The optimizer solves for 39 coefficients. Here, the longest period  $\tau$  is set to the length of the full data-blackout period.

The optimization algorithm converges to a solution with  $J = 10^{-5}$ . This solution, shown in Fig. 8, is not unique. There are multiple qualitatively different acceleration time histories that each reproduce the anomalous orbit change. Therefore, a physical explanation may exist. Furthermore, the direction of this force throughout the blackout period cannot be determined exactly from the information given.

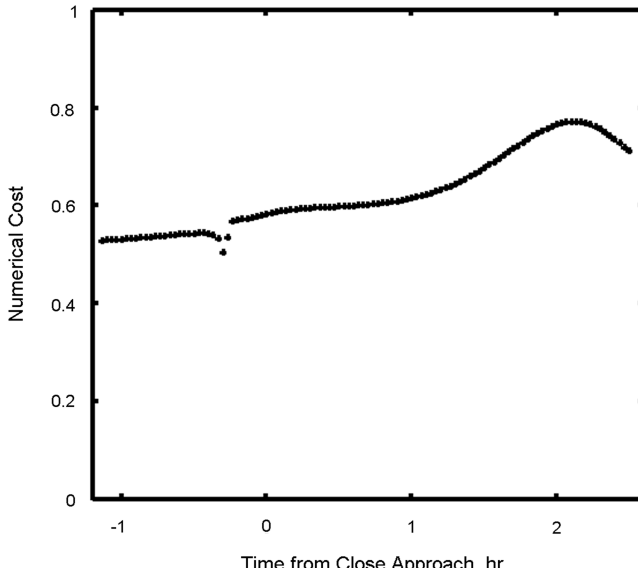


Fig. 9 Numerical cost at each optimized impulse time point.

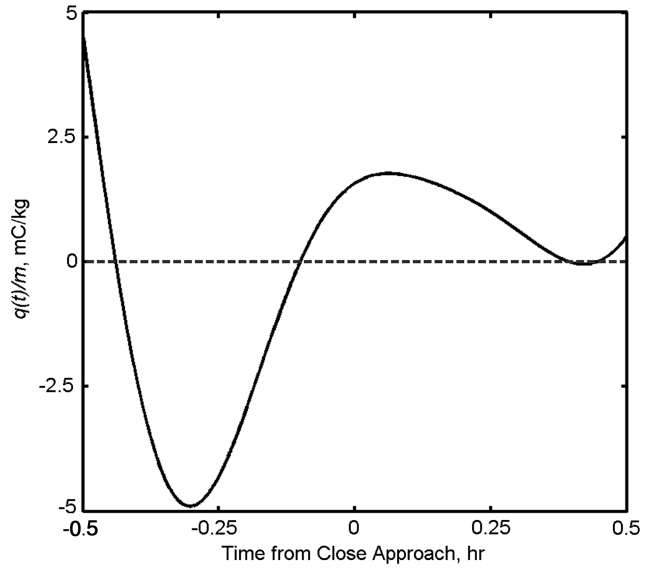


Fig. 10 Sample optimized  $q(t)/m$  time history.

It is possible that using this technique on other examples of the flyby anomaly can identify common trends among multiple spacecraft that may restrict the direction of the force. However, that issue is not pursued further in this study.

#### B. Possibility of a Single-Impulse Solution

Using the boxcar basis function instead of the more general Fourier series establishes whether or not an impulse can explain the anomaly. The simulation for this case uses three such functions with  $\Delta t = 10$  s to represent components in the  $\hat{r}$ ,  $\hat{\phi}$ , and  $\hat{\theta}$  directions. The optimizer varies three scalar parameters that define the magnitude and direction for each coordinate. The algorithm varies these three parameters in an effort to minimize the cost at the final state. The optimizer also includes a fourth parameter: the impulse start time. The optimizer runs for an array of start times spanning the blackout period, each two minutes apart.

The optimizer settles on impulses for which magnitudes are about  $10^{-4}$  to  $10^{-3}$  m/s<sup>2</sup>. The resulting costs, each associated with a single impulse at each time point, are shown in Fig. 9. They are decidedly nonzero, well above the error in the tracking. This result demonstrates that the unknown anomalous acceleration cannot be

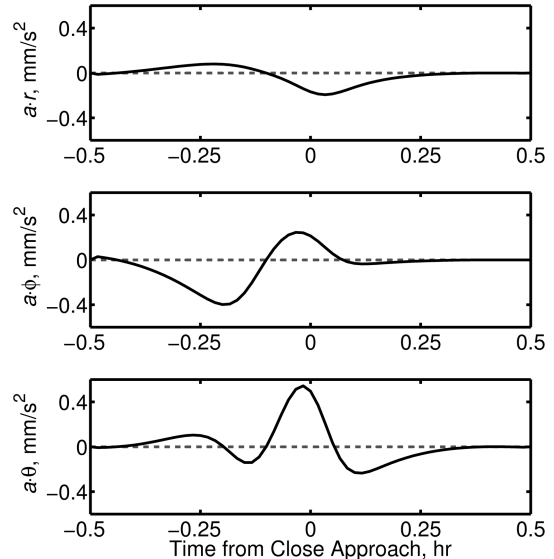


Fig. 11 Sample optimized Lorentz accelerations, shown in  $\hat{r}$ -,  $\hat{\phi}$ -, and  $\hat{\theta}$ -aligned components.

**Table 3** Normalized state errors

State	Error	Normalized error
$x$	6.7 m	7.7%
$y$	15.0 m	8.7%
$z$	<0.1 m	0.1%
$\dot{x}$	<0.1 mm/s	0.2%
$\dot{y}$	1.4 mm/s	20.2%
$\dot{z}$	24.2 mm/s	54.6%

attributed to a single impulsive event at some time in the blackout period. As a result of this analysis, the evaluation of the Lorentz force can neglect single-impulse  $q(t)$  time histories and focuses instead on continuous functions that can be approximated by the truncated Fourier series.

### C. Optimized Charge Time History

The optimization routine was initialized with each of the sample functions illustrated in Fig. 6 (units of  $\pm 10 \text{ mC/kg}$ ) as well as a zero vector. Each optimization run converged to a solution with  $J = 0.24$ , suggesting that none fully reproduces the anomaly. Although there are sometimes similarities between the solutions, it is difficult to identify any consistent features or qualities. Roughly speaking, each of the solutions is unique. Figure 10 shows one such optimized  $q(t)/m$  time history using both the maximum values of  $\tau$  and  $n$ . Figure 11 shows the corresponding acceleration in spherical coordinates. The individual state errors are normalized to  $\rho^0$  in Table 3, such that each value represents the fraction of anomalous error remaining after the charge time history has been applied. The error in  $\dot{z}$  clearly dominates the cost, with the supplied force accounting for only 50% of the anomalous change. To date, use of these algorithms and a Fourier basis function has not produced a more optimized solution.

## V. Conclusions

The Lorentz force satisfies all of the known properties of the Earth flyby anomaly. It is physical, nonconservative, bidirectional, distance-dependent, and dependent on declination. This research ignores the specific mechanisms by which a spacecraft could develop significant charge and, instead, treats charge as an output of the analysis. Focusing on the NEAR spacecraft's flyby, perturbation methods are employed to show that the required charge on the spacecraft would need to achieve both positive and negative values to produce the observed trajectory change.

Continuing with the NEAR flyby, numerical methods are used to search for a candidate charge time history. The solutions produced by this search can account for the orbit changes in some directions but, ultimately, no more than 75% of the change in an overall vector-magnitude sense. Although there exist continuous acceleration time histories that satisfy the observed state change, they cannot be associated with the Lorentz force alone. The optimized charge time histories cannot account for the state error in the  $z$  velocity. Therefore, it is unlikely that the anomaly can be attributed to an interaction of spacecraft charging with the geomagnetic field.

It turns out that  $v_{\infty}$  can be matched arbitrarily well if this single scalar is used as the only cost. The same is true for most other scalar cost functions, such as angular-momentum magnitude and energy in various frames. The reason is that the scalar nature of such a parameter obscures the more subtle vector mechanics of the problem. Therefore, the authors recommend that future work on the flyby anomaly consider the full orbital state to prevent false positives.

Although this study focuses on the Lorentz force, it makes at least two other more general contributions to the study of the flyby anomaly. First, the analysis allows one to conclude that the anomalous acceleration cannot be associated with a single impulse. Second, the numerical methodology described here is applicable to any physical phenomenon that can be represented as a time history for use in a simulation environment. It is likely that an exhaustive

reevaluation of the proposed causes of this anomaly using such a method, correlated across the many examples, will reveal more about the anomaly than is currently known.

### Acknowledgments

The authors wish to thank John D. Anderson of the Jet Propulsion Laboratory for providing insight and ephemerides throughout this research and Hans Feng of Cornell University for model validation analyses.

### References

- [1] Edwards, C., Stephens, S., Nandi, S., DiNardo, S., Border, J., Anderson, J., Nicholson, F., Bhaskaran, S., and Ottenhoff, C., "Tracking Galileo at Earth-2 Perigee Using the Tracking and Data Relay Satellite System," *Advances in the Astronautical Sciences*, Vol. 85, 1993, pp. 1609–1620; also American Astronautical Society Paper 93-685, 1993.
- [2] Anderson, J. D., Campbell, J. K., Ekelund, J. E., Ellis, J., and Jordan, J. F., "Anomalous Orbital-Energy Changes Observed during Spacecraft Flybys of Earth," *Physical Review Letters*, Vol. 100, No. 9, March 2008, Paper 091102. doi:10.1103/PhysRevLett.100.091102
- [3] Anderson, J. D., Campbell, J. K., and Nieto, M. M., "The Energy Transfer Process in Planetary Flybys," *New Astronomy Reviews*, Vol. 12, No. 5, July 2007, pp. 383–397. doi:10.1016/j.newast.2006.11.004
- [4] Lammerzahl, C., Preuss, O., and Dittus, H., "Is the Physics Within the Solar System Really Understood?," *Lasers, Clocks, and Drag-Free Control*, Springer-Verlag, Berlin, 2008, pp. 75–98.
- [5] Turyshev, S. G., and Toth, V. T., "The Puzzle of the Flyby Anomaly," *Space Science Reviews*, Vol. 148, Nos. 1–4, Aug. 2008, pp. 1–6. doi:10.1007/s11214-009-9571-0
- [6] Antreasian, P. G., and Guinn, J. R., "Investigations into the Unexpected Delta-V Increases During the Earth Gravity Assists of Galileo and NEAR," AIAA/AAS Astrodynamics Specialist Conference and Exhibit, Boston, MA, AIAA Paper 98-4287, Aug. 1998.
- [7] Hasse, W., Birsin, E., and Hänel, P., "On Force-Field Models of the Spacecraft Flyby Anomaly" [online archive], Feb. 2009, [http://arxiv.org/PS\\_cache/arxiv/pdf/0903/0903.0109v1.pdf](http://arxiv.org/PS_cache/arxiv/pdf/0903/0903.0109v1.pdf) [retrieved 11 Jan. 2010].
- [8] Lewis, R. A., "Field Theory Model of the Flyby Anomaly," *Space Propulsion and Energy Sciences International Forum (SPESIF-2009)*, AIP Conference Proceedings, Vol. 1103, American Inst. of Physics, Melville, NY, 2009, pp. 226–234. doi:10.1063/1.3115499
- [9] Busack, H. J., "Simulation of the Flyby Anomaly by Means of an Empirical Asymmetric Gravitational Field with Definite Spatial Orientation" [online archive], Nov. 2007, <http://fr.arxiv.org/ftp/arxiv/papers/0711/0711.2781.pdf> [retrieved 11 Jan. 2010].
- [10] Iorio, L., "The Effect of General Relativity on Hyperbolic Orbits and its Application to the Flyby Anomaly," *Scholarly Research Exchange*, Vol. 2009, 2009, Paper 807695. doi:10.3814/2009/807695
- [11] Cahill, R. T., "Resolving Spacecraft Earth-Flyby Anomalies with Measured Light Speed Anisotropy," *Progress in Physics*, Vol. 3, July 2008, pp. 9–15.
- [12] Cahill, R. T., "Combining NASA/JPL One-Way Optical-Fiber Light-Speed Data with Spacecraft Earth-Flyby Doppler-Shift Data to Characterise 3-Space Flow," *Progress in Physics*, Vol. 4, Oct. 2009, pp. 50–64.
- [13] Mbelek, J. P., "Special Relativity May Account for the Spacecraft Flyby Anomalies" [online archive], Sept. 2008, <http://arxiv.org/ftp/arxiv/papers/0809/0809.1888.pdf> [retrieved 11 Jan. 2010].
- [14] Gerrard, M. B., and Sumner, T. J., "Earth Flyby and Pioneer Anomalies" [online archive], Oct. 2008, [http://arxiv.org/PS\\_cache/arxiv/pdf/0807/0807.3158v2.pdf](http://arxiv.org/PS_cache/arxiv/pdf/0807/0807.3158v2.pdf) [retrieved 11 Jan. 2010].
- [15] Adler, S. L., "Can the Flyby Anomaly be Attributed to Earth-Bound Dark Matter?," *Physical Review D (Particles and Fields)*, Vol. 79, No. 2, 2009, Paper 023505. doi:10.1103/PhysRevD.79.023505
- [16] Adler, S. L., "Modeling the Flyby Anomalies with Dark Matter Scattering" [online archive], Aug. 2009, [http://arxiv.org/PS\\_cache/arxiv/pdf/0908/0908.2414v2.pdf](http://arxiv.org/PS_cache/arxiv/pdf/0908/0908.2414v2.pdf) [retrieved 11 Jan. 2010].
- [17] McCulloch, M. E., "Modeling the Flyby Anomalies Using a Modification of Inertia," *Monthly Notices of the Royal Astronomical Society: Letters*, Vol. 389, No. 1, July 2008, pp. L57–L60. doi:10.1111/j.1745-3933.2008.00523.x

- [18] McCulloch, M. E., "Can the Flyby Anomalies be Explained by a Modification of Inertia," *Journal of the British Interplanetary Society*, Vol. 61, Sept. 2008, pp. 373–378.
- [19] Petry, W., "A Possible Explanation of Anomalous Earth Flybys" [online archive], June 2008, <http://arxiv.org/abs/arXiv:0806.0334> [retrieved 11 Jan. 2010].
- [20] Grün, E., Kruger, H., Graps, A. L., Hamilton, D. P., Heck, A., Linkert, G., and et al., "Galileo Observes Electromagnetically Coupled Dust in the Jovian Magnetosphere," *Journal of Geophysical Research*, Vol. 103, No. E9, 1998, pp. 20011–20022. doi:10.1029/98JE00228
- [21] Colwell, J. E., Horanyi, M., and Grun, E., "Capture of Interplanetary and Interstellar Dust by the Jovian Magnetosphere," *Science*, Vol. 280, No. 5360, April 1998, pp. 88–91. doi:10.1126/science.280.5360.88
- [22] Schaffer, L., and Burns, J. A., "The Dynamics of Weakly Charged Dust: Motion Through Jupiter's Gravitational and Magnetic Fields," *Journal of Geophysical Research*, Vol. 92, No. A3, 1987, pp. 2264–2280. doi:10.1029/JA092iA03p02264
- [23] Horanyi, M., "Charged Dust Dynamics in the Solar System," *Annual Review of Astronomy and Astrophysics*, Vol. 34, No. 1, 1996, pp. 383–418. doi:10.1146/annurev.astro.34.1.383
- [24] Smith, B. A., Soderblom, L. A., Beebe, R. F., Boyce, J., Briggs, G. A., Bunker, A., and et al., "Encounter with Saturn: Voyager 1 Imaging Science Results," *Science*, Vol. 212, No. 4491, 1981, pp. 163–191. doi:10.1126/science.212.4491.163
- [25] Streetman, B., and M. Peck, "New Synchronous Orbits Using the Geomagnetic Lorentz Force," *Journal of Guidance, Control, and Dynamics*, Vol. 30, No. 6, 2007, pp. 1677–1690. doi:10.2514/1.29080
- [26] Streetman, B., and M. Peck, "A General Bang–Bang Control Method for Lorentz Augmented Orbits," *AAS Spaceflight Mechanics Meeting*, American Astronautical Society Paper 08-111, Galveston, TX, Jan. 2008, pp. 1–18.
- [27] Sumner, T., Araujo, H., Davidge, D., Howard, A., Lee, C., Rochester, G., Shaul, D., and Wass, P., "Description of Charging/ Discharging Process of the LISA Sensors," *Classical and Quantum Gravity*, Vol. 21, No. 5, March 2004, pp. S597–S602. doi:10.1088/0264-9381/21/5/031
- [28] Atchison, J. A., and Peck, M., "Lorentz Augmented Jovian Orbit Insertion," *Journal of Guidance, Control, and Dynamics*, Vol. 32, No. 2, March 2009, pp. 418–423. doi:10.2514/1.38406
- [29] Peck, M., Streetman, B., Saaj, C. M., and Lappas, V., "Spacecraft Formation Flying Using Lorentz Forces," *Journal of the British Interplanetary Society*, Vol. 60, No. 7, July 2007, pp. 263–267.
- [30] Streetman, B., and Peck, M., "Gravity-Assist Maneuvers Augmented by the Lorentz Force," *Journal of Guidance, Control, and Dynamics*, Vol. 32, No. 5, 2009, pp. 1639–1647. doi:10.2514/1.35676
- [31] Vallado, D. A., "General Perturbation Techniques," *Fundamentals of Astrodynamics and Applications*, 2nd ed., Microcosm Press, El Segundo, CA, 2004, pp. 567–669.